Electronic Supplementary Information (ESI) for

Overcoming the Limitations of Atomic-Scale Simulations on Semiconductor Catalysis with Changing Fermi Level and Surface Treatment

Seulgi Ji,[a] Dong Won Jeon,[b,c] Junghyun Choi,[d] Haneol Cho,[e] Bo-In Park,[f], Ilpyo Roh,[g] Hyungil Choi,[g] Chansoo Kim,[e] Jung Kyu Kim,[h] Uk Sim,[i] Danlei Li,[j] Hyunseok Ko,[k,] Sung Beom Cho,[b,c,*] and Heechae Choi,[a,j,*]*

[a]Institute of Inorganic Chemistry, University of Cologne, Greinstr. 6, Cologne, 50939, Germany

[b]Department of Materials Science and Engineering, Ajou University, Suwon, 16499 Republic of Korea

[c]Department of Energy Systems Research, Ajou University, Suwon, 16499 Republic of Korea

[d]Energy Storage Materials Center, Korea Institute of Ceramic Engineering and Technology (KICET), Jinju, Gyeongnam, 52851, Republic of Korea

[e]Korea Institute of Science and Technology (KIST), Hwrangro 14Gil 5, Seoul, Republic of Korea

[f]Department of Mechanical Engineering, Massachusetts Institute of Technology, Cambridge, MA, USA

[g]MO R&D Center, M.O.P Co., Ltd, Seoul, 07281, Republic of Korea

[h]School of Chemical Engineering, Sungkyunkwan University (SKKU), Suwon,16419 Republic of Korea

[i]Hydrogen Energy Technology Laboratory, Korea Institute of Energy Technology (KENTECH), Naju, 58330, Republic of Korea

[j]Department of Chemistry, Xi'an Jiaotong-Liverpool University, Suzhou, 215123, China

[k]Center of Material Digitalization, Korea Institute of Ceramic Engineering and Technology (KICET), Jinju, Gyeongnam, 52851, Republic of Korea

*Correspondence to: hko@kicet.re.kr (H. Ko), csb@ajou.ac.kr (S. B. Cho), heechae.choi@xjtlu.edu.cn (H. Choi)

Calculation methodology details

1. DFT Calculations

DFT calculations were performed using the Vienna ab initio package (VASP) with the projector augmented were method (PAW) to describe the interaction between valance and core electrons.(1–3) All DFT calculations were conducted with the general gradient approximation (GGA) with the Perdew-Burke-Ernzerhof (PBE) exchange-correlation functional.(4, 5) Optimization of cell parameters used a Gamma-centered *k*-point grids of 2 x 2 x 1 in cell for Brillouin zone sampling and a kinetic energy cut-off of 400 eV was used.(6) We used the DFT+U method, where the introduction of a Hubbard parameter U approximation modifies the self-interaction error and enhances the description of the on-site Coulomb interactions.(7) U_{eff} = 6 eV for Ce is employed to improve the description of the 4f states of Ce.(8) The energy convergence criteria in the self-consistent field were set to 10^{-6} eV and all geometry structures were fully relaxed until Hellman-Feynman forces achieved a range of 0.1 eV $Å^{-1}$. The supercell structure contains 135 items in lateral dimensions of 11.60 Å x 11.60 Å x 33.94 Å. A vacuum region of 20 Å was added to the substrate surface in the direction perpendicular to avoid interactions between the periodic slabs.

2. Details of the equation of Fermi level dependent adsorption energy

$$\Delta G_{ads} = \Delta E_0 + q(\varepsilon_F + E_{VBM}) + E_{iso} - E_{per} + q\Delta V + \Delta ZPE + \int C_p dT - T\Delta S \quad (2)$$

ΔE_0 in Eq 2 is the binding energy of adsorbates on CeO_2, which was obtained as follows,

$$\Delta E_0 = E_{ads/CeO_2} - E_{CeO_2} - \sum_i n_i \mu_i \quad (S1)$$

where E_{ads/CeO_2} and E_{CeO_2} in Eq S1 are the total energies of CeO_2 with and without the adsorbates, respectively, n_i is the number of atoms of species i (positive for reactant, negative for product), μ_i is the chemical potential of species i. The terms ΔZPE, $\int C_p dT$ and ΔS in Eq 2 mean the changes of zero-point energy, enthalpic, and entropy contributions at temperature T to a Gibbs free energy of an adsorbate, respectively. These three terms were calculated using harmonic vibrational frequencies of adsorbates bound to the substrate surface, on which the translational and rotational degrees of freedom of the adsorbate can be eliminated(9):

$$\Delta ZPE = \frac{1}{2}\sum \hbar\omega_i \quad (S2)$$

,

$$\int C_p dT = \sum_i \frac{\hbar\omega_i}{exp\left(\frac{\hbar\omega_i}{k_B T}\right) - 1} \quad (S3)$$

,

$$\Delta S = k_B \sum_i \left[\frac{\hbar\omega_i}{\exp\left(\frac{\hbar\omega_i}{k_B T}\right) - 1} - ln(1 - \exp\left(-\frac{\hbar\omega_i}{k_B T}\right)\right] \quad (S4)$$

where $\hbar$, ω_i, and k_B are the reduced Planck constant and ($\hbar = h/2\pi$), the vibrational frequency eigenvalue of *i*-th mode and Boltzmann constant, respectively.

A charged finite-cell is simulated by artificially introducing a compensating uniform background charge ("jellium background") to avoid the divergence in the electrostatic energy.

The formation energy of charged slab significantly depends on the supercell, especially on the vacuum thickness and charged states. Without correction, the formation energy will contain a non-negligible error.(10) Thus we corrected the formation energies of finite-size supercells with charged defects to eliminate the effects of the periodic boundary conditions by adding slab-based correction terms, $E_{iso} - E_{per} + q\Delta V$.(11, 12) E_{iso} is self-interaction of the isolated charge distribution; the energy of the model charge embedded in an infinite dielectric medium. E_{per} is the energy of the model charge embedded in the model dielectric medium under periodic boundary condition; both the self-interaction and the interaction with the periodic images and with the background charge. ΔV is the difference between the potential of the model charge system and DFT calculations. The correction term, $E_{iso} - E_{per} + q\Delta V,$ is assessed at two distinct vacuum thicknesses (10 and 25 Å). Subsequently, the corrected energies for charged adsorbates (E_{corr}) were validated by their substantial concordance (i.e., within 20 meV difference), as shown in Table S1.

Table S1. The uncorrected and corrected energetics for charged adsorbates across varying vacuum thicknesses.

species	$E_{uncorr} = \Delta E_0 + q(E_{VBM})$ [eV]		$E_{corr} = E_{uncorr} + E_{iso} - E_{per} + q\Delta V$ [eV]	
	Vacuum 10 Å	Vacuum 25 Å	Vacuum 10 Å	Vacuum 25 Å
$^*CH_3^+$	-2.89	-2.39	-3.07	-3.06
$^*CH_2^+$	1.70	2.19	1.56	1.56
$^*CH^+$	6.78	7.31	6.63	6.62
$^*CH_3^-$	4.41	4.87	4.33	4.34
$^*CH_2^-$	6.00	6.47	5.80	5.80
$^*CH^-$	5.31	5.79	5.11	5.11

Gibbs free energies of reaction (ΔG) for each of the reaction pathways were calculated with considerations of the partial pressure of produced H_2O (g) ($P_{H_2O\,(g)}$) in each reaction step depends on the amount of reactants. This assumption gives more reasonable local energetic landscape at each reaction step.

The partial pressure of produced $H_2O(g)$ ($P_{H_2O(g)}$) is dependent on the amount of reactants $CH_4(g)$ and $O_2(g)$, accordingly, we should consider the changeable $P_{H_2O(g)}$ to calculate Gibbs free energy of the reaction (ΔG).

$$\text{e.g. } CH_4(g) + aO_2(g) \rightarrow *Int + bH_2O(g) \quad \text{(R1)}$$

R1 is the reaction equation of methane oxidation producing the adsorbed intermediate (Int) and $H_2O(g)$ with $O_2(g)$ and $CH_4(g)$, where a and b are the coefficient of $O_2(g)$ and that of $H_2O(g)$. Regarding the reaction of adsorbates with $O_2(g)$, the equilibrium constant (K_P) can be derived relating to Boltzmann distribution,

$$K_p = \frac{{P_{H_2O(g)}}^b}{P_{CH_4(g)}\,{P_{O_2(g)}}^a} = exp(-\frac{\Delta}{k_B T}) \quad \text{(S5)}$$

where $P_{H_2O(g)}$, $P_{O_2(g)}$, k_B, and T and represent the partial pressure of H_2O and O_2, Boltzmann constant, and temperature, which was set to 923 K in this work. Δ is Gibbs free energy difference, which can be written as,

$$\Delta = \Delta G_{Int*} + b\,\mu_{H_2O(g)} - (\mu_{CH_4(g)} + a\,\mu_{O_2(g)}) \quad \text{(S6)}$$

where ΔG_{Int*} is related to Gibbs free energy of adsorption of intermediate. $\mu_{H_2O(g)}$, $\mu_{CH_4(g)}$, and $\mu_{O_2(g)}$ represent the chemical potential of $H_2O(g)$, $CH_4(g)$ and $O_2(g)$, respectively, which can be obtained by,

$$\mu_A(T,P) = E_A^{DFT} + \mu_A^o(T,P_A^o) + k_B T ln\frac{P_A}{P_A^o} \quad \text{(S7)}$$

where E_A^{DFT}, μ_A^o, and P_A are the total energy derived from DFT calculations, the standard chemical potential at the standard pressure P_A^o,(13) and the partial pressure of A at temperature T, respectively. $P_{H_2O(g)}{}^b$ in Eq S7 can be written as,

$$P_{H_2O(g)}{}^b = P_{CH_4(g)}\, P_{O_2(g)}{}^a \exp\left(-\frac{\Delta}{kT}\right) \tag{S8}$$

We can derive the equation relating Δ to $P_{H_2O(g)}$. Δ_0 is related to the difference of Gibbs free energy when $P_{H_2O(g)}$ is 1 atm and can be presented by,

$$\Delta_0 = \Delta G_{Int*} + b\mu_{H_2O(g)}^o - (\mu_{CH_4(g)} + a\,\mu_{O_2(g)}) \tag{S9}$$

$\mu_{H_2O(g)}^o$ is the chemical potential of H_2O at the standard states. Accordingly, Δ in Eq S6 and Δ_0 in Eq S9 can be written as using Eq S8,

$$\Delta = \Delta G_{Int*} + b(E_{DFT}^{H_2O} + \mu^o(T,P^o) + k_B T ln P_{H_2O(g)}) - (\mu_{CH_4(g)} + a\,\mu_{O_2(g)}) \tag{S10}$$

and

$$\Delta_0 = \Delta G_{Int*} + b(E_{DFT}^{H_2O} + \mu^o(T,P^o)) - (\mu_{CH_4(g)} + a\,\mu_{O_2(g)}) \tag{S11}$$

Thus, the difference between Δ and Δ_0 can be given by,

$$\Delta - \Delta_0 = bk_B T ln P_{H_2O(g)} \tag{S12}$$

Δ can be expressed as,

$$\Delta = \Delta_0 + bk_B T ln P_{H_2O(g)} \tag{S13}$$

Δ in Eq S18 can be substituted for Δ in Eq S13, accordingly, $P_{H_2O(g)}{}^b$ can be represented,

$$P_{H_2O(g)}{}^b = P_{CH_4(g)}\, P_{O_2(g)}{}^a \exp\left(-\frac{\Delta_0 + bk_B T ln P_{H_2O(g)}}{k_B T}\right) \tag{S14}$$

And $P_{H_2O(g)}{}^b$ can be rewritten as,

$$P_{H_2O(g)}{}^{b} = P_{O_2(g)}{}^{\frac{1}{4}}\exp\left(-\frac{\Delta_0}{k_BT}\right)\exp\left(-blnP_{H_2O(g)}\right) \quad \text{(S15)}$$

Thus, $P_{H_2O(g)}$ for the R1 is,

$$P_{H_2O(g)} = \left[P_{CH_4(g)}P_{O_2(g)}{}^{a}\exp\left(-\frac{\Delta_0}{k_BT}\right)\right]^{\frac{1}{2b}} \quad \text{(S16)}$$

Given that CH_4 (g) and O_2 (g) are introduced into the chamber first, it was assumed that the active sites on CeO_2 surface were taken by reaction intermediates and oxygen competitively. Accordingly, at first the adsorption energies of *CH_4 and *O were calculated to check whether the reactants contribute to the reaction as a gas phase itself or adsorbed phase on the surface. We set the pressure of CH_4 (g) and O_2 (g) to 0.2 Torr (≈ 0.00026 atm) and 1 Torr (≈ 0.0013 atm) in this work, which is the reaction condition from the literature.(14) To calculate the adsorption energy of CH_4 (g) and O_2 (g), the chemical potentials of gas phase molecules A were obtained by using the following equation,

$$\mu_A(T,P) = E_A^{DFT} + \mu_A^o(T,P_A^o) + k_BTln\frac{P_A}{P_A^o} \quad \text{(S17)}$$

where E_A^{DFT}, μ_A^o, and P_A in Eq S17 are the total energy derived from DFT calculations, the standard chemical potential at the standard pressure P_A^o,(13) and the partial pressure of gas-phase A molecules A at temperature T, respectively.

3. Charge states of intermediates

***CH_4:** only neutral CH_4 was considered because four valence electrons of C atom are bonded with four H atoms by sp^3 hybridization.

***CH_3:** two adsorption configurations were considered: vertical and horizontal. Because the horizontal adsorption configuration was thermodynamically more favored than the vertical configuration, the adsorption energies of horizontally adsorbed CH_3 were considered to calculate the Gibbs free energy. Since CH_3 has one radical in p orbital, +1, -1, and 0 charge states were considered. Neutral CH_3 was not adsorbed on the CeO_2 surface.

***CH_2:** CH_2 has one empty p orbital and one lone pair of electrons, thus, they can behave as an electron acceptor and donor. Accordingly, charge states of +2, +1, -1, and -2 were considered. +2 charged CH_2 (q = +2) was not adsorbed, because CH_2O molecule was formed with O atom from CeO_2 surface.

***CH:** CH has either one or three unpaired electrons, depending on the molecule's excitation state. We only considered one radical of CH with +1, 0, and -1 charge states to calculate the adsorption energy.

***C:** The electron configuration of C is $1s^2 2s^2 2p^2$, in which C has two half-filled and one unoccupied 2p orbitals, so we considered +2, +1, and -1 charge states. C with charge state +2 was not adsorbed.

***CHO**: Since C has a radical, behaving electron donor or acceptor, +1, -1, and 0 were considered. CHO^+ with a linear molecular geometry was not adsorbed on the surface.

***OCHO:** O atom of OCHO has one radical and two lone pairs, thus, we considered charge states of -1, +1, and 0.

***CO:** C and O atoms, which are bonded with triple bonds each other, obey the octet rule for both molecules. Therefore, only neutral CO was considered.

***CO_2:** C and two O atoms are bonded with double bonds and each atom obeys the octet rule. Only neutral CO_2 was considered.

***O:** The electron configuration is $1s^2 2s^2 2p^4$ with one fully filled and two half-filled 2p orbitals, so we considered +1, -1, and -2 charge states. However, the adsorption of *O charged with +1 was found to be highly unstable.

4. Methane oxidation reaction pathway

We investigated three representative reaction pathways of methane oxidation with O_2 (g) as shown in Scheme S1.(15)

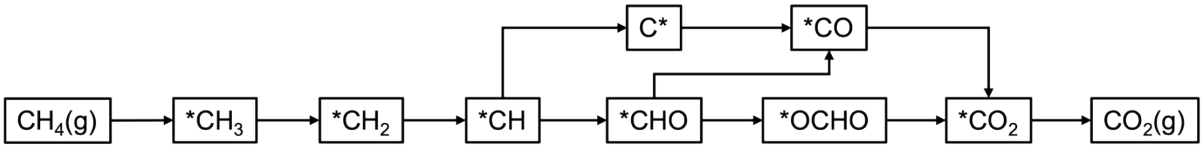

Scheme S1. The considered reaction pathway of methane oxidation.

Pathway mediated by the intermediates C* with O_2(g):

$CH_4(g) \rightarrow *CH_3 \rightarrow *CH_2 \rightarrow *CH \rightarrow *C \rightarrow *CO \rightarrow *CO_2 \rightarrow CO_2(g)$

Pathway mediated by the intermediates *CHO with O_2(g):

$CH_4(g) \rightarrow *CH_3 \rightarrow *CH_2 \rightarrow *CH \rightarrow *CHO \rightarrow *CO \rightarrow *CO_2 \rightarrow CO_2(g)$

Pathway mediated by the intermediates *OCHO with O_2(g):

$CH_4(g) \rightarrow *CH_3 \rightarrow *CH_2 \rightarrow *CH \rightarrow *CHO \rightarrow *OCHO \rightarrow *CO_2 \rightarrow CO_2(g)$

In addition, we considered the reaction pathway with O*.

Pathway with O*:

$CH_4(g) \rightarrow *CH_2 \rightarrow *C \rightarrow *CO \rightarrow *CO_2 \rightarrow CO_2(g)$

Elementary reaction steps (R2~R12) of methane oxidation with O_2 (g) are listed below,

$$CH_4(g) + \frac{1}{4}O_2(g) \rightarrow *CH_3 + \frac{1}{2}H_2O(g) \quad (R2)$$

$$*CH_3 + \frac{1}{4}O_2(g) \rightarrow *CH_2 + \frac{1}{2}H_2O(g) \quad (R3)$$

$$*CH_2 + \frac{1}{4}O_2(g) \rightarrow *CH + \frac{1}{2}H_2O(g) \quad (R4)$$

$$*CH + \frac{1}{4}O_2(g) \rightarrow *C + \frac{1}{2}H_2O(g) \quad (R5)$$

$$*CH + \frac{1}{2}O_2(g) \rightarrow *CHO \quad (R6)$$

$$*C + \frac{1}{2}O_2(g) \rightarrow *CO \quad (R7)$$

$$*CHO + \frac{1}{4}O_2(g) \rightarrow *CO + \frac{1}{2}H_2O(g) \quad (R8)$$

$$*CHO + \frac{1}{2}O_2(g) \rightarrow *OCHO \quad (R9)$$

$$*OCHO + \frac{1}{4}O_2(g) \rightarrow *CO_2 + \frac{1}{2}H_2O(g) \quad (R10)$$

$$*CO + \frac{1}{2}O_2(g) \rightarrow *CO_2 \quad (R11)$$

$$*CO_2 \rightarrow CO_2(g) + * \quad (R12)$$

5. The surface reaction rate ratio

The surface Fermi level ($\varepsilon_F(r)$) is dependent on the difference between the bulk Fermi level of CeO_2 ($\varepsilon_{F(CeO_2)}$) and the degree of band bending ($eV_{BB}(r)$), thus, we can represent as,

$$\varepsilon_F(r) = \varepsilon_{F(CeO_2)} - eV_{BB}(r) \quad \text{(S18)}$$

The contact potential ($V_{BB}(r_{cocat})$) at the interface can be obtained by,

$$V_{BB}(r_{cocat}) = (\phi_{cocat} - \phi_{semi})/e \quad \text{(S19)}$$

where the work function of a cocatalyst (ϕ_{cocat}) and that of semiconductor (ϕ_{semi}), respectively. r_{cocat} is the radius of a cocatalyst. In a cocatalyst/semiconductor catalyst system, a hemispherical cocatalyst NP with a size of less than 10 nm is generally loaded on a semiconductor surface. We employed a mathematical model of a partially embedded spherical cocatalyst NP in a semiconductor with a finite interface by editing an embedded spherical cocatalyst NP/a semiconductor model, which was proposed by Ioannides and Verykios.(16) Accordingly, the Poisson equation in the three-dimensional form must be employed for a finite interface between a metal NP with a small size and a semiconductor instead of the one-dimensional form for an infinite cocatalyst/semiconductor interface model.(16, 17)

$$\nabla^2 V_{BB}(x,y,z) = -\frac{\rho}{\varepsilon_r \varepsilon_0} = -\frac{\rho}{\varepsilon} \quad \text{(S20)}$$

where ρ, ε_r, and ε_0 in Eq S20 present the space charge density, the relative dielectric constant of CeO_2, which is 23, and the vacuum permittivity ($8.854 \times 10^{-12} C \cdot V^{-1} m^{-1}$), respectively. $\varepsilon_r \varepsilon_0$ is the permittivity of the medium and is denoted by ε. The electric field (E(r)) within the depletion region ($r_{cocat} \leq r \leq r_{cocat} + D$, D is the depletion layer thickness) between a hemispherical cocatalyst and a semiconductor (3D) can be,

$$E(r) = \frac{eN_d}{3\varepsilon}((r_{cocat} + D)^3 - r^3) \quad (r_{cocat} \leq r \leq r_{cocat} + D) \quad \text{(S21)}$$

Accordingly, the electric potential (V_{BB}) can be obtained as follows,

$$V_{BB}(r) = \frac{eN_d}{6\varepsilon}\left(\frac{D^2}{2} - \frac{r^2}{6} - \frac{D^3}{3r}\right) \quad (r_{cocat} \leq r \leq r_{cocat} + D) \quad \text{(S22)}$$

$$V_{BB} = 0 \quad (r > r_{cocat} + D) \quad \text{(S23)}$$

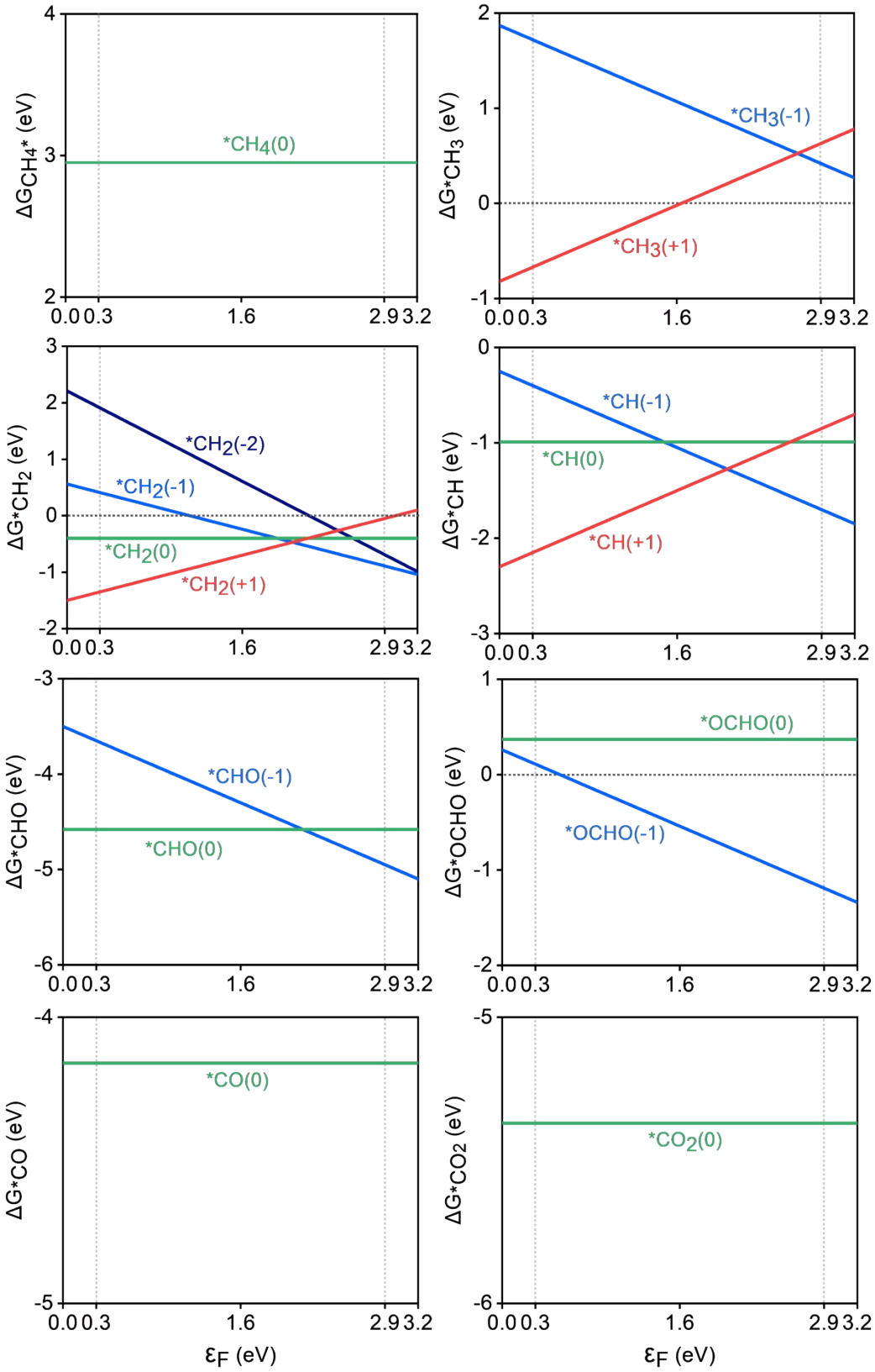

Fig. S1 The graph of Gibbs free adsorption energy of the reaction.

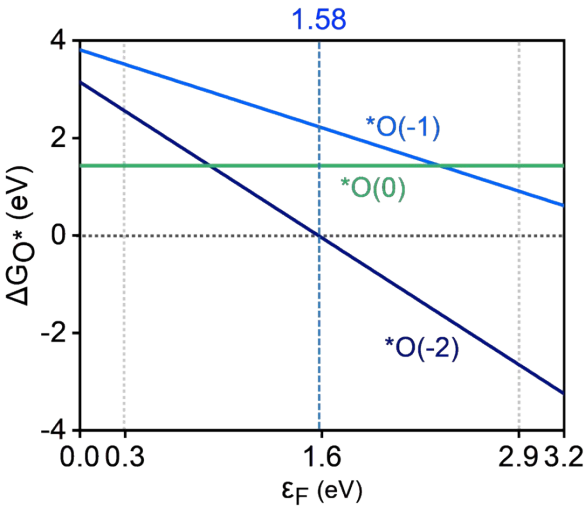

Fig. S2 The Gibbs free energy of *O adsorption as a function of Fermi level at 925 K.

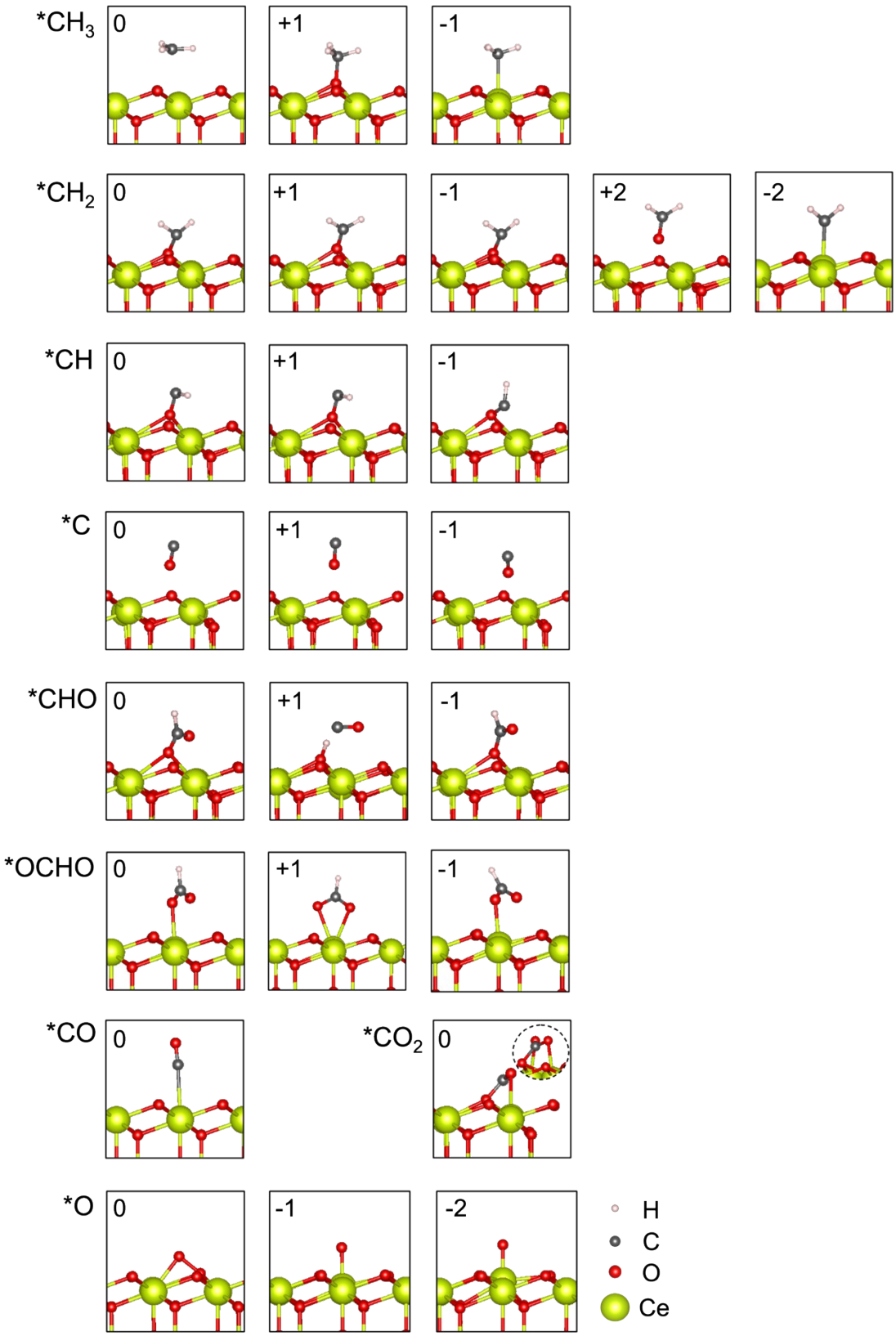

Fig. S3 The optimized configurations of adsorbates. The numbers inside the boxes represent the charge state, q.

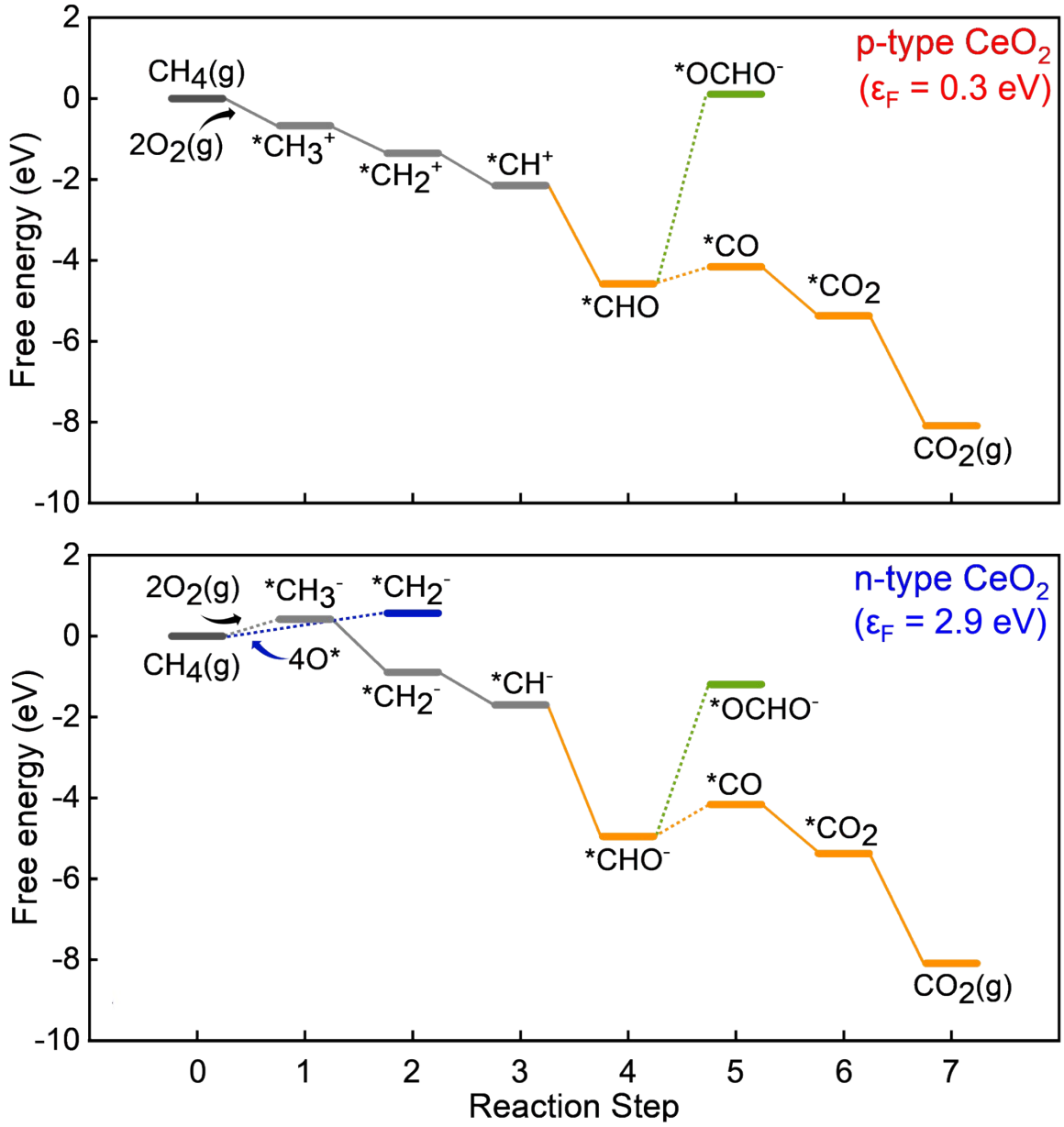

Fig. S4 Free energy diagrams of methane oxidation on the p-type (ε_F = 0.3 eV) and the n-type (ε_F = 2.9 eV) CeO_2. Solid and dashed lines represent the free energy downhill and uphill, respectively. Grey lines: methane dissociation, Orange lines: *CHO-mediated pathway with O_2 (g), Green lines: *OCHO-mediated pathway with O_2 (g), Blue line: pathway with O*.

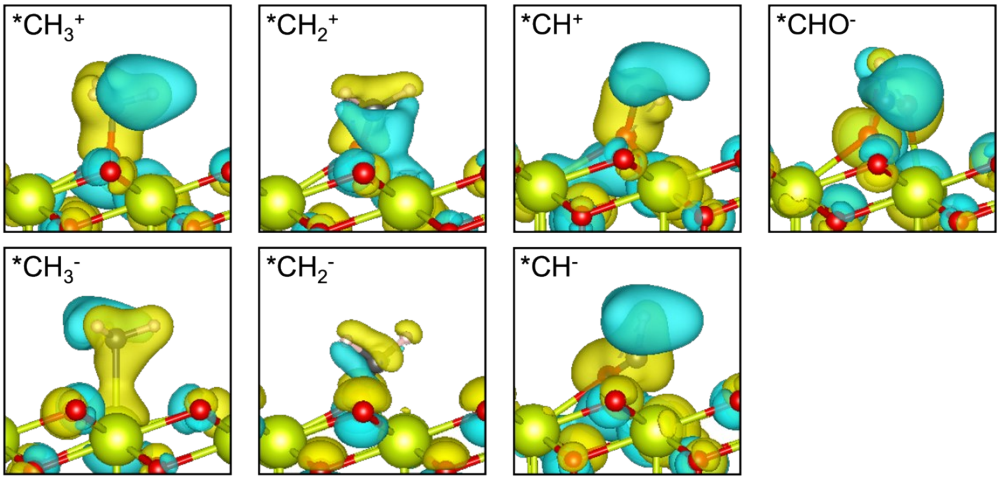

Fig. S5 Charge density difference plots of CH_3, CH_2, CH, C, and CHO on a CeO_2 surface. The yellow and cyan blue regions denote the electron accumulation and depletion regions, respectively. The isovalue is 0.20 e/Bohr.

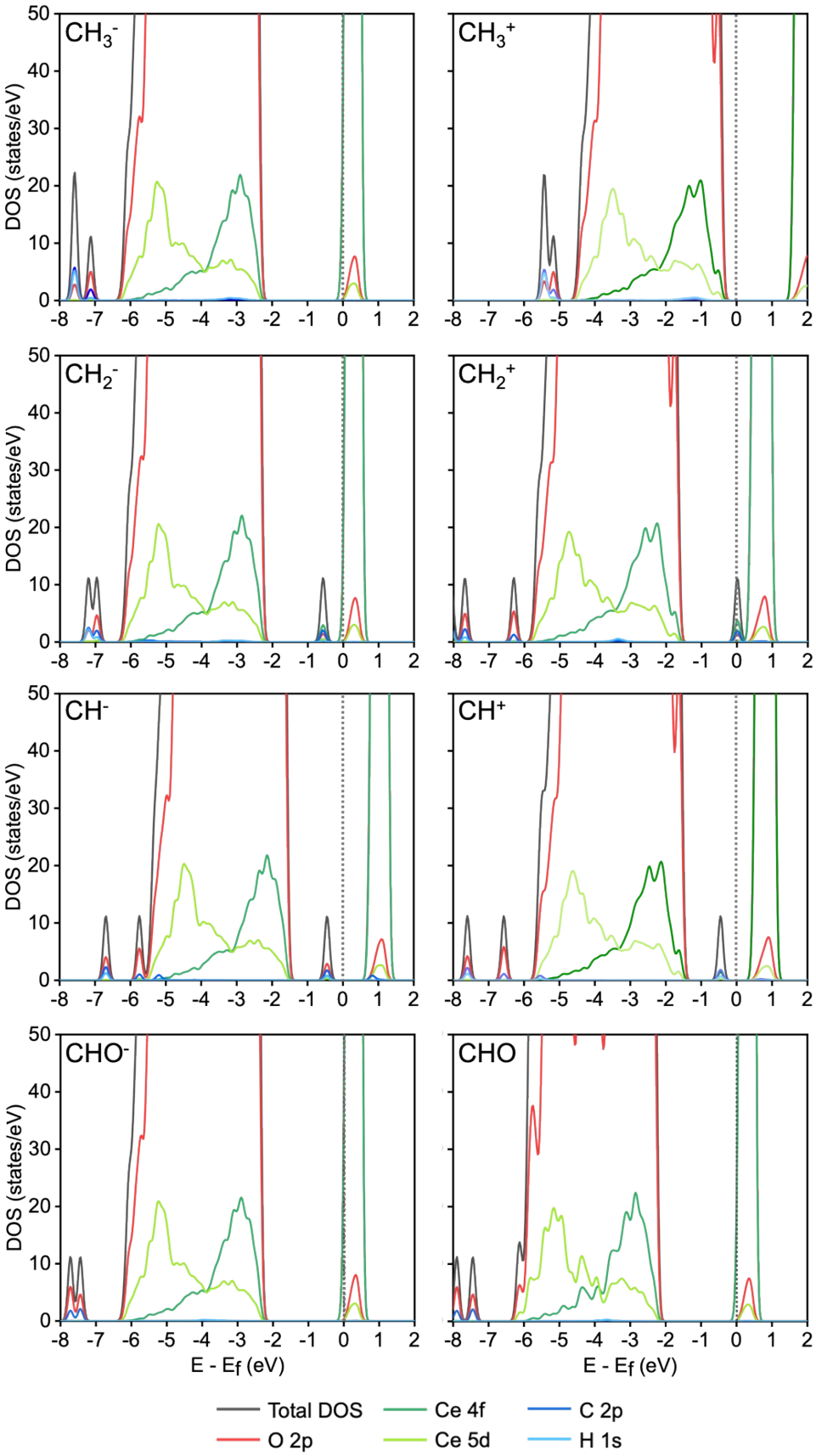

Fig. S6 Density of states (DOS) of CH_3, CH_2, CH, and CHO intermediates.

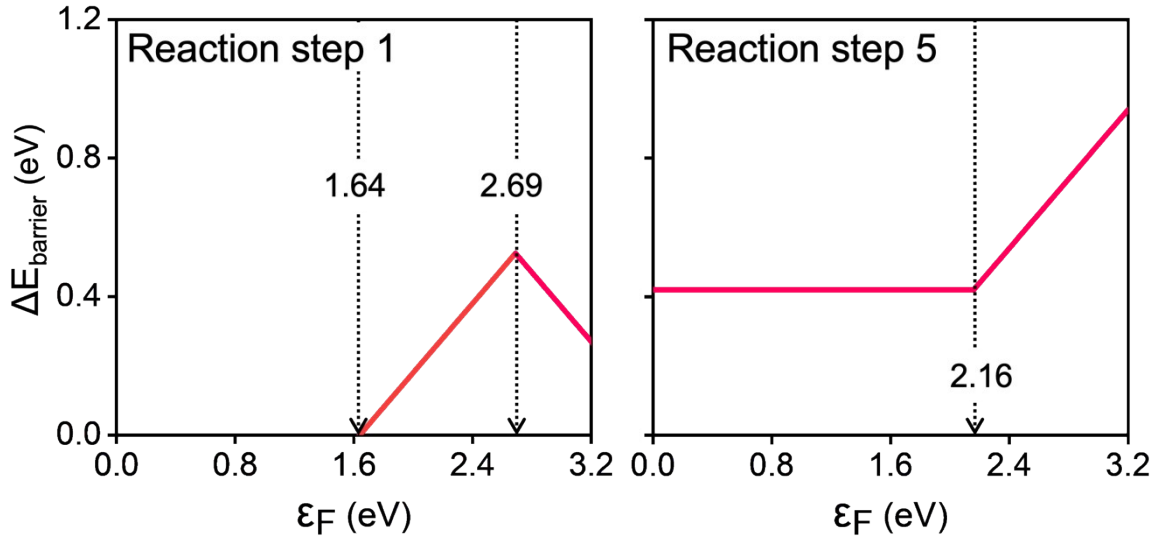

Fig. S7 The energy barrier graphs of reaction step 1 and reaction 5 as a function of the Fermi level of CeO_2.

The reaction step 1:

$$CH_4(g) + ¼O_2 \rightarrow *CH_3^+ + ½H_2O(g)\ (1.64 \leq \varepsilon_F\,(eV) < 2.69)$$

$$CH_4(g) + ¼O_2 \rightarrow *CH_3^- + ½H_2O(g)\ (2.69 \leq \varepsilon_F\,(eV))$$

The reaction step 5:

$$*CHO + ¼O_2 \rightarrow *CO + ½H_2O(g)\ (\varepsilon_F\,(eV) < 2.16)$$

$$*CHO^- + ¼O_2 \rightarrow *CO + ½H_2O(g)\ (2.16 \leq \varepsilon_F\,(eV))$$

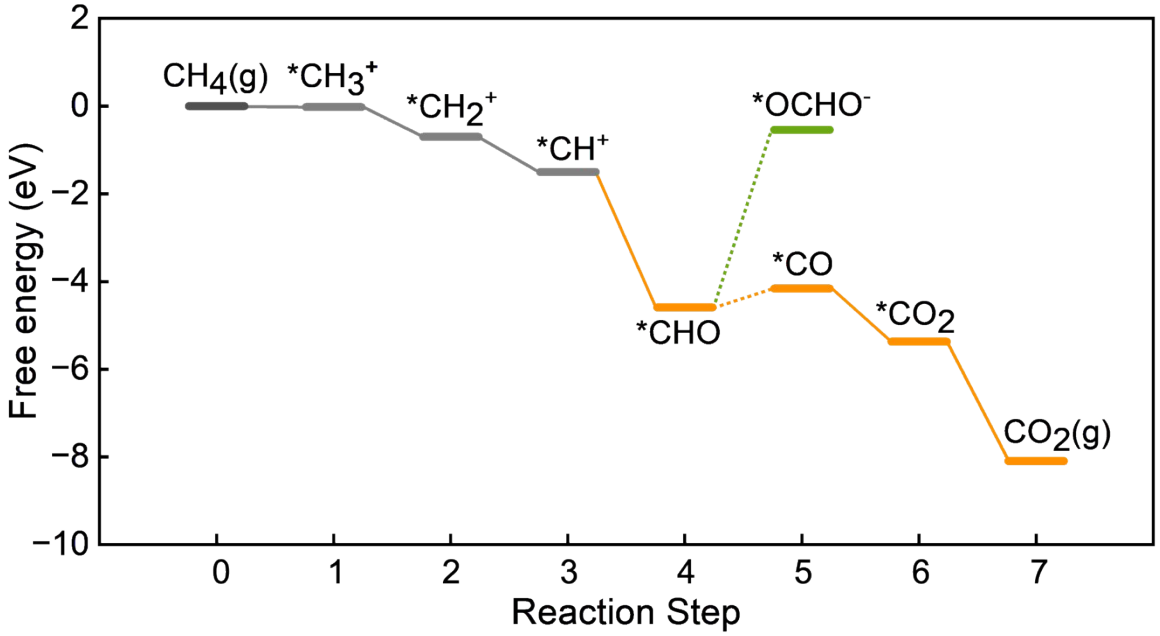

Fig. S8 Free energy diagram at Fermi level (0 eV ~ 1.64 eV) with the lowest value of energy barrier.

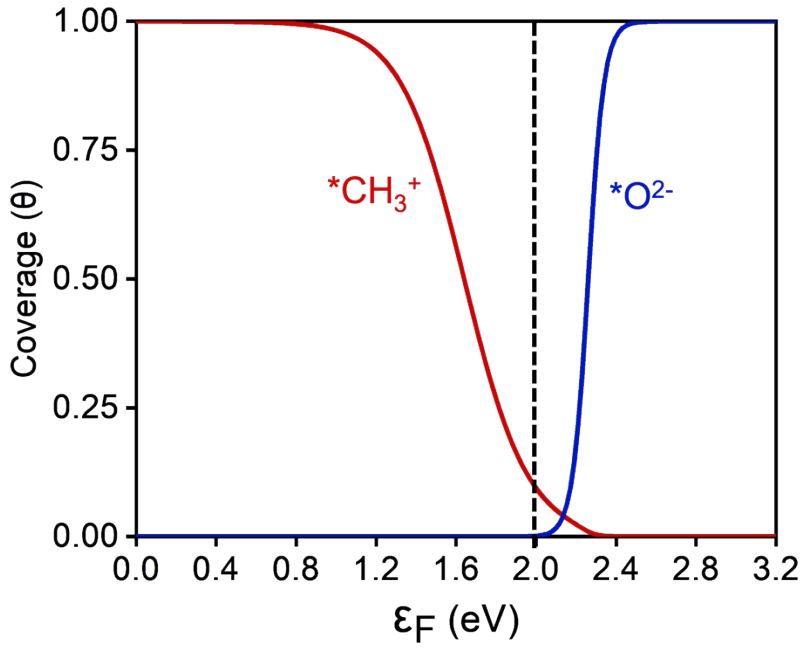

Fig. S9 The graph of the coverage of *CH_3 and *O as a function of Fermi level. We considered the coverage of *CH_3 for θ_{ads} term because *CH_3 is a key intermediate to initiate methane oxidation with O_2 (g) in the first reaction step. This process competes with *O^{2-} adsorption. As the Fermi level of CeO_2 increases, the coverage of *CH_3 decreases, while *O^{2-} occupies most of the active sites. This graph was obtained by using the following equations,

$$\theta_{*CH_3} = \frac{e^{-\frac{\Delta G_{*CH_3}}{kT}}}{1 + e^{-\frac{\Delta G_{*O}}{kT}} + e^{-\frac{\Delta G_{*CH_3}}{kT}}} \quad \text{(S24)}$$

$$\theta_{*O} = \frac{e^{-\frac{\Delta G_{*O}}{kT}}}{1 + e^{-\frac{\Delta G_{*O}}{kT}} + e^{-\frac{\Delta G_{*CH_3}}{kT}}} \quad \text{(S25)}$$

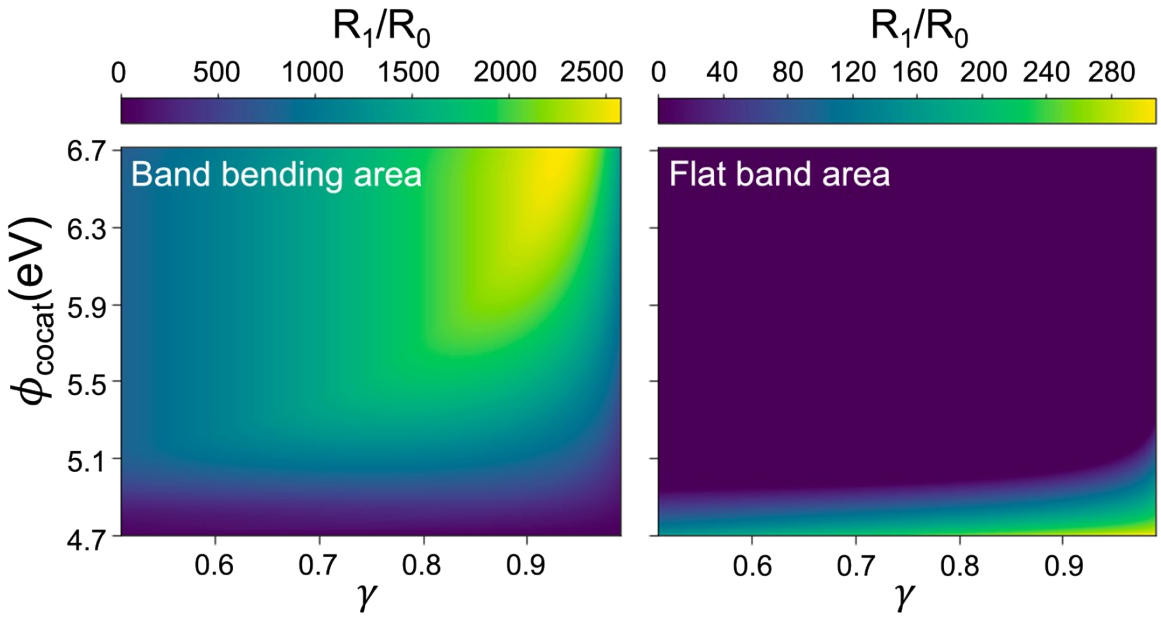

Fig. S10 The contour map of surface reaction rate constant ratio (R_1/ R_0) of a cocatalyst/CeO_2 (R_1) to that of bulk CeO_2 without a cocatalyst (R_0) of band bending area and flat band area (N_d = 10^{19} cm^{-3}), respectively.

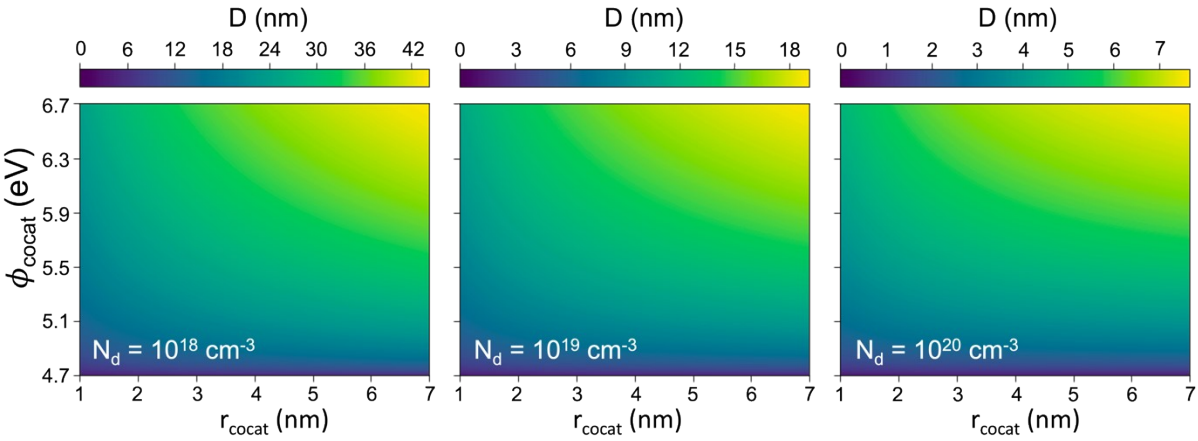

Fig. S11 The graph of depletion region width as a function of a cocatalyst radius (r_{cocat}) and cocatalyst work function ($\emptyset_{cocat}$).

References

1. G. Kresse, J. Furthmüller, Efficiency of ab-initio total energy calculations for metals and semiconductors using a plane-wave basis set. *Computational Materials Science* **6**, 15–50 (1996).

2. G. Kresse, D. Joubert, From ultrasoft pseudopotentials to the projector augmented-wave method. *Phys. Rev. B* **59**, 1758–1775 (1999).

3. G. Kresse, J. Furthmüller, Efficient iterative schemes for *ab initio* total-energy calculations using a plane-wave basis set. *Phys. Rev. B* **54**, 11169–11186 (1996).

4. J. P. Perdew, K. Burke, M. Ernzerhof, Generalized Gradient Approximation Made Simple. *Phys. Rev. Lett.* **77**, 3865–3868 (1996).

5. J. P. Perdew, *et al.*, Atoms, molecules, solids, and surfaces: Applications of the generalized gradient approximation for exchange and correlation. *Phys. Rev. B* **46**, 6671–6687 (1992).

6. H. J. Monkhorst, J. D. Pack, Special points for Brillouin-zone integrations. *Phys. Rev. B* **13**, 5188–5192 (1976).

7. S. L. Dudarev, G. A. Botton, S. Y. Savrasov, C. J. Humphreys, A. P. Sutton, Electron-energy-loss spectra and the structural stability of nickel oxide: An LSDA+U study. *Phys. Rev. B* **57**, 1505–1509 (1998).

8. S.-W. Yu, *et al.*, Energy levels of the Ce activator relative to the YAP(Ce) scintillator host. *J. Phys.: Condens. Matter* **27**, 185501 (2015).

9. J. Kleis, *et al.*, Trends for Methane Oxidation at Solid Oxide Fuel Cell Conditions. *J. Electrochem. Soc.* **156**, B1447 (2009).

10. H.-P. Komsa, T. Rantala, A. Pasquarello, Comparison between various finite-size supercell correction schemes for charged defect calculations. *Physica B: Condensed Matter* **407**, 3063–3067 (2012).

11. H.-P. Komsa, A. Pasquarello, Finite-Size Supercell Correction for Charged Defects at Surfaces and Interfaces. *Phys. Rev. Lett.* **110**, 095505 (2013).

12. M. Farzalipour Tabriz, B. Aradi, T. Frauenheim, P. Deák, SLABCC: Total energy correction code for charged periodic slab models. *Computer Physics Communications* **240**, 101–105 (2019).

13. M. W. Chase, *et al.*, JANAF Thermochemical Tables, 1982 Supplement. *Journal of Physical and Chemical Reference Data* **11**, 695–940 (1982).

14. J. Dou, *et al.*, Complete Oxidation of Methane on Co3O4/CeO2 Nanocomposite: A Synergic Effect. *Catalysis Today* **311**, 48–55 (2018).

15. R. Wang, *et al.*, Mechanism of the catalytic oxidation of methane on Pt(1 1 1) surfaces in moist environment: A density functional theory study. *Applied Surface Science* **471**, 566–586 (2019).

16. T. Ioannides, X. E. Verykios, Charge Transfer in Metal Catalysts Supported on Doped TiO2: A Theoretical Approach Based on Metal–Semiconductor Contact Theory. *Journal of Catalysis* **161**, 560–569 (1996).

17. Z. Zhang, J. T. Yates, Band Bending in Semiconductors: Chemical and Physical Consequences at Surfaces and Interfaces. *Chem. Rev.* **112**, 5520–5551 (2012).